

WHAT PREVENTS INTERNAL GRAVITY WAVES FROM DISTURBING THE SOLAR UNIFORM ROTATION?

Pavel A. Denissenkov^{1,2}, Marc Pinsonneault¹, and Keith B. MacGregor³

ABSTRACT

Internal gravity waves (IGWs) are naturally produced by convection in stellar envelopes, and they could be an important mechanism for transporting angular momentum in the radiative interiors of stars. Prior work has established that they could operate over a short enough time scale to explain the internal solar rotation as a function of depth. We demonstrate that the natural action of IGWs is to produce large scale oscillations in the solar rotation as a function of depth, which is in marked contrast to the nearly uniform rotation in the outer radiative envelope of the Sun. An additional angular momentum transport mechanism is therefore required, and neither molecular nor shear-induced turbulent viscosity is sufficient to smooth out the profile. Magnetic processes, such as the Tayler-Spruit dynamo, could flatten the rotation profile. We therefore conclude that IGWs must operate in conjunction with magnetic angular momentum transport processes if they operate at all. Furthermore, both classes of mechanisms must be inhibited to some degree by mean molecular weight gradients in order to explain the recent evidence for a rapidly rotating embedded core in the Sun.

Subject headings: stars: interiors — Sun: rotation — waves

1. Introduction

During their pre-main sequence contraction, young solar-type stars are spun up to rotational velocities of the order of 100 km s^{-1} . However, during their subsequent main sequence

¹Department of Astronomy, The Ohio State University, 4055 McPherson Laboratory, 140 West 18th Avenue, Columbus, OH 43210; dpa@astronomy.ohio-state.edu, pinsono@astronomy.ohio-state.edu.

²On leave from Sobolev Astronomical Institute of St. Petersburg State University, Universitetsky Pr. 28, Petrodvorets, 198504 St. Petersburg, Russia.

³High Altitude Observatory, National Center for Atmospheric Research, P.O. Box 3000, Boulder, CO 80307-3000; kmac@hao.ucar.edu.

(MS) evolution the surface rotation slows down as a result of angular momentum loss through magnetized stellar winds (Kawaler 1988; Matt & Pudritz 2008). If a convective envelope and a radiative core of a solar-type MS star rotated independently of one another then the surface spindown would lead to a strong differential rotation beneath the envelope. In contradiction with this, helioseismic data (e.g., Couvidat et al. 2003) reveal that the solar radiative core rotates as a solid body and almost synchronously with the convective envelope at least down to the radius $r \approx 0.2 R_{\odot}$. Besides, the spindown of young cluster stars (Stauffer & Hartmann 1987; Keppens et al. 1995; Bouvier et al. 1997; Krishnamurthi et al. 1997; Barnes 2003) requires that the internal differential rotation only persists for timescales of the order of 20 Myr to 100 Myr. These data indicate that, in radiative interiors of solar-type MS stars, there is an efficient mechanism of angular momentum redistribution that couples their core and envelope rotation. Unfortunately, its physical nature remains elusive in spite of many attempts to understand it made in the last years. Matters are further complicated by the requirement that an appropriate model of angular momentum transport in the solar-type MS stars should also reproduce the intricate variations (depletion) of the surface Li abundance as functions of age and effective temperature observed in the same stars (Sestito & Randich 2005).

A breakthrough in solving this complex problem has recently been announced by Talon & Charbonnel (2005) and Charbonnel & Talon (2005). They have shown how internal gravity waves (hereafter, IGWs) generated by the envelope convection can extract angular momentum from rapidly rotating radiative cores of the solar-type MS stars on short enough timescales to explain both the spindown of young cluster stars and the quasi-solid-body rotation of the Sun. Furthermore, they have found that the quick flattening of the internal rotation profile by IGWs reduces element diffusion coefficients associated with hydrodynamic instabilities induced by differential rotation to values consistent with those constrained by the Li data.

Pursuing the goal of uncovering intrinsic causes of canonical extra mixing in low-mass red giant branch stars (Denissenkov & Vandenberg 2003) and trying to understand the origin of fast rotation of red horizontal branch stars (Sills & Pinsonneault 2000), we have been undertaking a critical review of different transport mechanisms in stellar radiative zones. When applying our test model of angular momentum redistribution by IGWs to a model of the present-day Sun, we have found that IGWs strongly disturb the solar internal rotation making it disagree with the helioseismic data. The disturbance can be eliminated only if there is another transport mechanism competing with IGWs. Its efficiency should exceed that of the rotational shear mixing used by Talon & Charbonnel (2005) by more than three orders of magnitude. Alternatively, a magnetic transport mechanism could be a competitor for IGWs. But in that case the mechanism preventing IGWs from disturbing the solid-body rotation of the Sun could itself be responsible for both shaping the internal rotation of the

solar-type MS stars and assisting in the depletion of their surface Li abundance. This paper presents a discussion of computational results that support our conclusions.

2. Angular Momentum Transport by IGWs

In a gravitational field, any perturbation exerted on a fluid excites in it both acoustic (p-modes) and internal gravity waves (g-modes). The driving force for the latter is the buoyancy, as opposed to the pressure for the p-modes. A general discussion of their combined linear theory can be found in the book by Lighthill (1978). Our application of the IGW theory first addresses the following three questions: How do IGWs propagate through radiative layers? How do they redistribute angular momentum in a rotating star? How are IGWs generated? Answering the last question necessarily includes a discussion of the IGW spectrum. We start with general comments on IGWs, then attempt to examine the underlying issues.

The physics of angular momentum transport and chemical mixing by IGWs in stellar radiative zones has been comprehensively described by Press (1981), García López & Spruit (1991), Zahn et al. (1997), Ringot (1998), Kumar et al. (1999), Montalbán & Schatzman (2000), Kim & MacGregor (2001), Talon et al. (2002), and Talon & Charbonnel (2005). In all of these papers, IGWs are considered to be generated by large-scale turbulent fluid motions either in the convective envelope or at the interface between the radiative core and convective envelope. The net energy flux of IGWs at the core/envelope interface r_c is usually estimated as $F_E(r_c) \approx \mathcal{M}_t F_c$, where $F_c = \rho_c v_c^3 \approx 0.1 (L/4\pi r_c^2)$ is the convective flux, L is the star’s luminosity, and $\mathcal{M}_t = \omega_c/N_c$ is the turbulent Mach number. In the last ratio, N_c is the buoyancy frequency immediately beneath the interface, while $\omega_c = 2\pi v_c/\lambda_c$ is the turnover frequency of the largest convective eddy approaching the interface with the velocity v_c . Everywhere in this paper ω denotes the circular frequency. Although it should be measured in rad s^{-1} , we will always express its values in units of μHz , assuming that $1 \mu\text{Hz} \equiv 10^{-6} \text{ rad s}^{-1}$. In the mixing-length theory (MLT) of convection, that we apply, the diameter of the largest turbulent eddy, which also measures its mean free path λ_c , is an α_{MLT} fraction of the local pressure scale height H_P . We employ the stellar evolution code described by Denissenkov et al. (2006). Gravitational settling is not included because it does not affect the IGW propagation. Indeed, IGWs can easily penetrate inner radiative cores of low-mass MS stars (Talon & Charbonnel 2005) where radial variations of the mean molecular weight μ are much stronger than those incurred from the operation of gravitational settling. We use the Grevesse & Noels (1993) mixture of heavy elements. Our calibrated solar model reproduces the solar luminosity ($L_\odot = 3.85 \times 10^{33} \text{ erg s}^{-1}$) and radius ($R_\odot = 6.96 \times 10^{10} \text{ cm}$) at the solar age of 4.57 Gyr; this procedure yields the helium and heavy-element mass frac-

tions $Y = 0.273$, $Z = 0.018$, and the mixing length α_{MLT} of 1.75. Our solar model has $r_c \approx 0.713 R_\odot$ and $\mathcal{M}_{t,\odot} \approx 8.3 \times 10^{-4}$, so that the energy luminosity of IGWs at the bottom of its convective envelope $L_E(r_c) = 4\pi r_c^2 F_E(r_c)$ comprises only $\sim 0.0083\%$ of L_\odot .

On their way from the bottom of the convective envelope toward the center of a solar-type MS star, IGWs experience radiative damping. This can be taken into account by applying a wave attenuation factor $\exp(-\tau)$ to $L_E(r_c)$. To calculate the effective optical depth, we use the relation

$$\tau = [l(l+1)]^{3/2} \int_r^{r_c} K \frac{NN_T^2}{\sigma^4 \sqrt{1 - (\sigma/N)^2}} \frac{dr'}{r'^3} \quad (1)$$

derived by Zahn et al. (1997). Here, $N^2 = N_T^2 + N_\mu^2$, where

$$N_T^2 = \frac{g\delta}{H_P} (\nabla_{\text{ad}} - \nabla_{\text{rad}}), \quad \text{and} \quad N_\mu^2 = g\varphi \left| \frac{\partial \ln \mu}{\partial r} \right|$$

are the T - and μ -component of the square of the buoyancy frequency. In the last two expressions, ∇_{rad} and ∇_{ad} are the radiative and adiabatic temperature gradients (logarithmic and with respect to pressure), and g is the local gravity. The quantities $\delta = -(\partial \ln \rho / \partial \ln T)_{P,\mu}$ and $\varphi = (\partial \ln \rho / \partial \ln \mu)_{P,T}$ are determined by the equation of state. In our IGW computations, the equation of state for the ideal gas is used. In this particular case, $\delta = \varphi = 1$. Also in equation (1), $K = 4acT^3 / 3\kappa\rho^2 C_P$ is the radiative diffusivity with κ and C_P representing the Rosseland mean opacity and the specific heat at constant pressure, respectively. The quantities l and σ are introduced below.

Turbulent eddies with different length and overturn time scales present in the convective envelope can generate a whole spectrum $S_E(r_c, l, m, \omega)$ of IGWs with different spherical degrees $l \geq 1$, azimuthal numbers m ($|m| \leq l$), and frequencies ω . If the star rotates and its angular velocity Ω varies with r then the optical depth (1) depends on all three of the wave's spectral characteristics, the latter two entering it through the doppler-shifted frequency $\sigma = \omega - m[\Omega(r) - \Omega(r_c)]$ (we use a cartesian coordinate system in which the z-axis is colinear with the vector $\mathbf{\Omega}$). Values of this frequency should be watched to remain between 0 and N . When $\sigma \rightarrow 0$, the optical depth τ approaches the infinity, and the wave is completely absorbed by the surrounding medium. On the other hand, when $\sigma \rightarrow N$, the wave is totally reflected back (Ringot 1998). If only the IGWs with $1 \leq l \leq l_{\text{max}}$ and $\omega_{\text{min}} \leq \omega \leq \omega_{\text{max}}$ are excited and propagate into the radiative core then their net energy flux at the core/envelope interface is

$$F_E(r_c) = \sum_{l=1}^{l_{\text{max}}} \sum_{m=-l}^l \int_{\omega_{\text{min}}}^{\omega_{\text{max}}} S_E(r_c, l, m, \omega) d\omega = \mathcal{M}_t F_c. \quad (2)$$

Besides energy, IGWs can also carry angular momentum the flux of which is

$$F_J = \frac{m}{\sigma} F_E \quad (3)$$

(Ringot 1998; Kumar et al. 1999). Since both F_E and σ are positive, this relation means that prograde waves (those with $m > 0$) carry positive angular momentum while retrograde waves ($m < 0$) transport negative momentum. Note that before Ringot’s elucidating paper the improper (negative) sign was used in equation (3) by many researchers creating some confusion in the field.

Let us choose a frame of reference co-rotating with the convective envelope and denote $\Delta\Omega(r) \equiv \Omega(r) - \Omega(r_c)$. We will assume that, in spite of the action of the Coriolis force in this noninertial frame of reference, the spectrum of IGWs generated by the envelope convection is still axisymmetric, i.e. $S_E(r_c, l, m, \omega) = S_E(r_c, l, -m, \omega)$; if necessary, corrections due to the Coriolis force can be taken into account later on (e.g., Talon & Charbonnel 2003). If $\Delta\Omega(r) = 0$, i.e. if the whole star rotates uniformly, then $\sigma = \omega$, and τ does not depend on m . In this case, the total angular momentum luminosity associated with IGWs

$$L_J(r) = 4\pi r_c^2 \sum_{l=1}^{l_{\max}} \sum_{m=-l}^l m \int_{\omega_{\min}}^{\omega_{\max}} S_E(r_c, l, m, \omega) \exp\{-\tau(r, l, m, \omega)\} \frac{d\omega}{\omega} \quad (4)$$

is equal to zero at any radius r below the convective envelope.

On the other hand, if $\Delta\Omega(r) \neq 0$, i.e. if the star rotates differentially, then IGWs will experience selective damping in the radiative core. Indeed, let us assume for example that $\Delta\Omega(r)$ increases with depth (when r decreases). In this case, the frequency σ of a prograde wave with spectral characteristics l , m , and ω will be doppler shifted to values smaller than the intrinsic frequency ω , while that of a retrograde wave with the characteristics l , $-m$ and ω will become larger than ω as the waves propagate inward. Hence, the difference between their attenuation factors $\exp\{-\tau(r, l, m, \omega)\} - \exp\{-\tau(r, l, -m, \omega)\}$ will diminish with the depth. This happens because the prograde waves carrying the positive angular momentum experience stronger damping (if $\Delta\Omega(r) > 0$) on their way into the radiative core than the retrograde waves carrying the negative angular momentum. The positive angular momentum absorbed by the surroundings at the beginning of the waves’ path will spin up rotation locally compared to $\Omega(r_c) + \Delta\Omega$ while the negative momentum accumulating in the waves as they advance inward will be deposited deeper where the retrograde waves get eventually absorbed. This briefly sketched physics of angular momentum redistribution by IGWs is incorporated into the following PDE:

$$\rho r^2 \frac{\partial \Delta\Omega}{\partial t} = \frac{1}{r^2} \frac{\partial}{\partial r} \left(\rho r^4 \nu \frac{\partial \Delta\Omega}{\partial r} \right) + \frac{3}{8\pi} \frac{1}{r^2} \frac{\partial L_J}{\partial r}, \quad (5)$$

where ν is a viscosity. Supplemented with eqs. (1), (4), an expression for the IGW spectrum at $r = r_c$, and appropriate initial and boundary conditions, this equation describes how the star’s internal rotation profile evolves in the presence of IGWs and a viscous force.

3. Spectra of IGWs

Given that the optical depth τ , that determines the efficiency of damping of an IGW, strongly depends on the wave’s spectral characteristics l , m , and ω , knowing the spectral energy distribution for IGWs at the core/envelope interface is as important as estimating their net energy. In this paper, we will use two analytical prescriptions (eqs. 6 and 7 below) for the spectra of IGWs. They correspond to two different physical mechanisms of the IGW excitation by turbulence in the convective envelope. The formal lower and upper limits for the intrinsic frequency of these IGWs are $\omega_{\min} = \omega_c$ and $\omega_{\max} = N_c$.

Unfortunately, multidimensional hydrodynamic simulations of turbulent convection in the solar envelope and its penetration into the radiative core give contradictory results on the spectrum of IGWs generated in these numerical experiments. For example, in their 2D simulations Rogers & Glatzmaier (2005) have found an IGW energy flux evenly distributed in frequency at least for $l \leq 20$ with a peak energy that is three orders of magnitude smaller than that predicted by equation (7). On the other hand, Kiraga et al. (2005) claim that the broad frequency IGW spectrum reported in their earlier publication was an artefact of the 2D approximation. They emphasize that the IGW flux obtained in their new 3D simulations is of the same order as the one calculated from the simple parametric model of García López & Spruit (1991) based on the MLT. This finding encourages us to use spectrum (6) as our primary IGW model.

3.1. The García López & Spruit Spectrum

This prescription approximates the spectrum of IGWs generated at the core/envelope interface as a result of dynamic hitting at the radiative side of the interface by breaking convective eddies. This approximation was proposed and developed by Press (1981), García López & Spruit (1991), and Zahn et al. (1997). We use an expression derived in the last work

$$S_E(r_c, l, m, \omega) = \frac{1}{2} \rho_c v_c^3 \frac{\omega_c}{N_c} \frac{1}{l_c \omega_c} \left(\frac{\omega_c}{\omega} \right)^3 \frac{1}{2l}. \quad (6)$$

Equation (6) is obtained under the following assumptions: (i) the dynamic pressure in the waves of a frequency ω matches that produced by the convective eddies with the overturn

time $\sim \omega^{-1}$; (ii) the kinetic energy spectrum of the convective motions in the envelope is represented by the Kolmogorov law; (iii) besides waves at their own length scale λ , the convective eddies also excite IGWs with horizontal wave lengths $\lambda_h > \lambda$ by the superposition of their incoherent action on the interface; these longer waves have a velocity amplitude reduced by the factor λ/λ_h (García López & Spruit 1991). In this prescription, $l_{\max} = l_c(\omega/\omega_c)^{3/2}$, where $l_c = 2\pi r_c/\lambda_c$. Applying the integration and summation (2) to the spectrum (6) and noticing that $\omega_c \ll N_c$, we find that $F_E(r_c) = \mathcal{M}_t F_c$ as expected.

3.2. The Goldreich et al. Spectrum

The second prescription originated from the investigation of the stochastic excitation of p-modes by turbulent convection in the Sun carried out by Goldreich et al. (1994). In this model, IGWs are generated by the fluctuating Reynolds stresses produced by turbulent fluid motions in the convective envelope. Following Talon et al. (2002), the emerging IGW spectrum at the core/envelope interface can be estimated as

$$S_E(r_c, l, m, \omega) = \frac{1}{2l} \frac{\omega^2}{4\pi} \int_{r_c}^{R_c} dr \frac{\rho^2}{r^2} \left[\left(\frac{\partial \xi_r}{\partial r} \right)^2 + l(l+1) \left(\frac{\partial \xi_h}{\partial r} \right)^2 \right] \times \exp \left[-l(l+1) \frac{h_\omega^2}{2r^2} \right] \frac{v^3 \lambda^4}{1 + (\omega \tau_\lambda)^{15/2}}, \quad (7)$$

where R_c is the outer radius of convective envelope, $\tau_\lambda = \lambda/v$ is the overturn time of convective elements of the size $\lambda = \alpha_{\text{MLT}} H_P$ moving with the velocity v (at $r = r_c$, λ and v coincide with the parameters λ_c and v_c defined in §2), and $h_\omega = \lambda \min\{1, (2\omega\tau_\lambda)^{-3/2}\}$. Like equation (6), the latter equation has been derived under the assumption that the turbulent motions in the convective envelope obey the Kolmogorov law.

The radial displacement wave function ξ_r and the horizontal one $l(l+1)\xi_h$, the latter being related to the former by the continuity equation (Zahn et al. 1997), are normalized to the unit IGW energy flux just below the convection zone. For the radial function, we use the WKB solution (Press 1981; Zahn et al. 1997; Kumar et al. 1999)

$$\xi_r(r) = C[l(l+1)]^{1/4} \frac{\exp \left[- \int_{r_c}^r \frac{|N|}{\omega} \frac{\sqrt{l(l+1)}}{r'} dr' \right]}{\omega(\rho r |N|)^{1/2}}. \quad (8)$$

This equation shows that in the convective envelope, where $N^2 < 0$, IGWs are evanescent. Therefore only those of them that are excited close to the core/envelope interface will effectively contribute to the IGW flux at $r = r_c$. The constant C is adjusted in our computations

for the spectrum (7) to yield $F_E(r_c) = \mathcal{M}_t F_c$ with $F_c = 0.1 (L/4\pi r_c^2)$. The factor $(2l)^{-1}$ in eqs. (6) and (7) takes into account the assumed energy equipartition between the wave counterparts with opposite signs of the azimuthal number ($-l \leq m \leq l$).

In Fig. 1, we have plotted the logarithms of the IGW energy luminosity summed over all available values of m at the core/envelope interface in our solar model. Those were calculated using the spectra (6) (solid curve) and (7) (dashed curves) with the same value of $\mathcal{M}_t = 8.3 \times 10^{-4}$ that gives $L_E(r_c) \approx 3.2 \times 10^{29} \text{ erg s}^{-1}$. Apparently, they have quite different dependences on the spherical degree and frequency. Whereas the first spectrum does not depend on l at all¹ (eq. 6), the second is estimated to be proportional to l^p , where $p \approx 1.6$ for the first 4 degrees. Besides, the first spectrum declines with increasing ω much slower (with a power -3) than the second spectrum (with a power ~ -4.5). As a result, in the second case the dipole wave ($l = 1$), that experiences the least damping (eq. 1), carries much less energy toward the radiative core than it does in the first case, especially at higher frequencies (compare the lower dashed and solid curve).

3.3. Uncertainties in the MLT

Fig. 2 shows how the convective and buoyancy frequency, ω_c and N , vary with the radius on the opposite sides of the core/envelope interface in our solar model. From this figure, it is evident that neither the minimum frequency of IGWs $\omega_{\min} = \omega_c$ nor the ratio $\mathcal{M}_t = \omega_c/N_c$ estimating the net energy flux $F_E(r_c) \approx \mathcal{M}_t F_\odot$ (dotted curve in the figure shows that the latter approximation becomes valid at $r \gtrsim r_c + 0.5H_P$), can be predicted with a confidence by the MLT of convection employed by us. The uncertainties are caused by the rapid growth of ω_c and N with an increasing distance from the interface. Strictly speaking, both $\omega_c \propto v_c$ and $N \propto |\nabla_{\text{rad}} - \nabla_{\text{ad}}|^{1/2}$ should vanish at $r = r_c$. However, as soon as we step aside from the interface, both of them jump up to finite values. In stellar model computations, their first nonzero values depend on spatial resolution: the higher the resolution is, the smaller these values are. For example, in our computations of the present-day Sun’s model, the results of which are plotted in Fig. 2, we find $\omega_c \approx 0.30 \mu\text{Hz}$ and $N_c \approx 360 \mu\text{Hz}$, hence $\mathcal{M}_t \approx 8.3 \times 10^{-4}$. If we had taken into account convective overshooting beyond the formal lower boundary of convective envelope located at the radius $r = r_c$, where $\nabla_{\text{rad}} = \nabla_{\text{ad}}$ (the Schwarzschild criterion), then we would have obtained a larger value of N_c . In a value of $\mathcal{M}_t = \omega_c/N_c$, the increase of N_c due to the overshooting can partly be compensated by choosing a larger representative value of ω_c that should account of its rapid growth with radius on a length

¹The factor $(2l)^{-1}$ disappears after the summation over all $m = -l, \dots, l$.

scale much less than H_P immediately above the core/envelope interface (dashed curve).

Besides the aforementioned uncertainties in the choice of representative values for ω_c and N_c , the MLT does not account for the fact, established by laboratory experiments, observations in the Earth’s atmosphere and numerical simulations (e.g., see Stein & Nordlund 1989; Cattaneo et al. 1991; Rieutord & Zahn 1995; Montalbán & Schatzman 2000; Rogers & Glatzmaier 2006), that downward flows in a strongly stratified convection zone are much more energetic and confined in their horizontal extent than upward flows. This may result in an underestimate of the IGW net energy flux, especially in stars with deep convective envelope, like the Sun (Kiraga et al. 2005).

Given the uncertainties in the MLT and the fact that we want to investigate the stability of the solar uniform rotation against perturbations by the IGWs that were supposed to be powerful enough to produce that uniform rotation in the past, we tentatively choose $\omega_{\min} = \omega_c = 0.30 \mu\text{Hz}$ while considering the turbulent Mach number \mathcal{M}_t as a free parameter with its minimum value equal to our estimated ratio $\omega_c/N_c \approx 8.3 \times 10^{-4}$. This may actually put a conservative lower limit on the energetics of such IGWs because other authors, including Charbonnel & Talon (2005) who demonstrated how the IGWs could shape the Sun’s uniform rotation, employed larger values of \mathcal{M}_t and sometimes also a higher ω_{\min} . Therefore, their low-degree high-frequency waves, that can penetrate deep into the radiative core, carried more kinetic energy than they do in our basic case, assuming, of course, that we use the same IGW spectrum. For the convective parameter l_c , we use an MLT value $l_c = 30$ from our calibrated solar model.

4. Qualitative Description of Expected Solutions

After the proper (positive instead of negative) sign in relation (3) had been defined by Ringot (1998) it became clear that the addition of IGWs to other processes responsible for the redistribution of angular momentum in stellar radiative zones would not be a trivial problem. Indeed, instead of resulting in an exponential decay of perturbations of the internal rotation profile toward a solid body rotation (e.g., Kumar & Quataert 1997), the damping of IGWs leads to progressively growing deviations of local rotation from its initial state, even if this state is close to the solid body rotation. This is caused by the fact that in a region rotating faster than the convective envelope the prograde waves experience stronger damping than the retrograde waves, which results in a deposit of positive angular momentum there and hence in a further spin-up of this region. The opposite is true for a region rotating slower than the convective envelope. Of course, the perturbations of the rotation profile cannot grow infinitely large. First of all, an excess of (positive or negative) angular momentum in

them can slowly be dissipated through the molecular viscosity. Second and more important, when the rotational shear produced by the perturbations becomes strong enough to trigger a shear instability the turbulent viscous friction associated with the shear-induced turbulence will start to contribute to smoothing the perturbations out.

Apparently, the outcome of the competition between the disturbing action of IGWs and the smoothing effect of viscous friction depends on their relative strength. Let us take a constant viscosity $\nu = \nu_0$. It is obvious that, as long as ν_0 is kept extremely large, the rotation profile will remain stationary because any perturbation of Ω by IGWs will be quickly neutralized by the viscous dissipation. Of course, this does not preclude gradual temporal changes of the rotation profile as a whole due to the redistribution of angular momentum by IGWs as described by eq. (5).

If we begin to decrease ν_0 then at some critical value of it, which is proportional to the local IGW energy flux, regular oscillations of Ω will set in. In the Earth’s atmosphere, this bifurcation of a stationary solution toward an oscillatory solution is believed to be observed experimentally as the quasi-biennial oscillations (QBO) of the mean zonal wind in the equatorial stratosphere disturbed by IGWs coming down from the troposphere (e.g., Lindzen & Holton 1968; Plumb 1977; Yoden & Holton 1988). In models of the solar-type MS stars, a behavior of the Ω -profile resembling that of the QBO has been found as a solution of equation (5) near the top of radiative core by Kumar et al. (1999); Kim & MacGregor (2001); Talon et al. (2002); Talon & Charbonnel (2003), and Charbonnel & Talon (2005). Talon & Charbonnel (2005) have called it the shear layer oscillations (SLOs). They have proposed that the SLOs work as a filter for IGWs on their way toward the radiative core. If Ω increases with the depth in the core, as is expected in a solar-type MS star losing its angular momentum from the surface through a magnetized stellar wind, then the SLOs predominantly filter out the retrograde waves. These are absorbed closer to the center. Possessing the minimum angular momentum, it is the very central part of the core that slows down the first. Following it, increasingly more and more distant from the center layers get successively decelerated (Talon & Charbonnel 2005). Note, however, that this theoretical prediction has recently been challenged by results of a preliminary analysis of the GOLF data on solar g-mode oscillations reported by García et al. (2007). They suggest that the solar inner core at $r \lesssim 0.15 R_\odot$ may rotate three to five times as fast as the rest of the radiative zone. If these results are confirmed by a further analysis they will likely rule out the angular momentum redistribution in the Sun by IGWs.

If we continue to reduce ν_0 further on then the oscillations will grow up in amplitude until finally they will turn into chaotic variations of Ω (e.g., Kim & MacGregor 2001).

5. Results: Two Spectra, Five Viscosities

In this section, we present and discuss results of our numerical solutions of the PDE (5) that have been obtained with the IGW spectra (6) and (7) using the viscosity prescriptions summarized in Appendix B. Besides restricting the azimuthal number m by the values of $\pm l$, we have also considered a limited set of the spherical degree. In most of our computations, we have only used a set of numbers $l = 1, 2, 3$, and 4 . We do not think that adding higher degrees would qualitatively change our results and conclusions. Indeed, the optical depth in the wave attenuation factor $\exp(-\tau)$ increases as $\tau \propto l^3$ for $l > 1$, therefore at a same radius in the Sun’s radiative core a contribution to the local energy flux of a wave with a higher l is made from a part of the spectrum at a higher frequency $\omega \sim l^{3/4}$ (solid curves in Fig. 3). As both of the IGW spectra quickly decline with a growth of ω , our neglect of waves with the higher spherical degrees is unlikely to lead to a serious mistake. The same argument justifies our choice of the limited frequency interval $0.3 \mu\text{Hz} \leq \omega \leq 3 \mu\text{Hz}$ because waves with higher frequencies transport negligible amounts of kinetic energy and angular momentum.

Unlike the other papers cited in the preceding section, in this work we have not tried to solve the full problem of shaping the uniform rotation of the solar radiative core by IGWs. A tentative solution of it has been provided by Charbonnel & Talon (2005). We look at this problem from another perspective. Let us assume that the redistribution of angular momentum in the Sun’s core has already established its solid body outer envelope rotation as revealed by the helioseismic data (e.g., Couvidat et al. 2003). Despite this, IGWs still continue to be generated by the envelope convection. We cannot expect *a priori* that the stability of the Ω -profile against perturbations by IGWs strongly depends on its shape. Therefore, we consider it worth investigating whether these perturbations are sufficiently weak in the present-day Sun for them not to disturb noticeably the Sun’s uniform rotation, provided that the IGWs producing these perturbations had enough energy in the past to couple the Sun’s core and envelope rotation. Given our reformulation of the problem, we have chosen the following initial and boundary conditions for eq. (5):

$$\Delta\Omega(0, r) = \frac{r_c - r}{r_c - r_b} \Delta\Omega(0, r_b) \quad \text{for } r_b \leq r \leq r_c, \quad (9)$$

$$\text{and } \Delta\Omega(t, r_c) = 0, \quad \Delta\Omega(t, r_b) = \Delta\Omega(0, r_b), \quad (10)$$

where $r_b = r_c - 0.6 R_\odot$. Thus, we assume that $\Delta\Omega$ initially increases with the depth linearly up to its maximum value $\Delta\Omega(0, r_b)$. Taking into account that for the present-day Sun $\Omega(r_c) \approx 2.9 \mu\text{Hz}$, the initial rotational shear in our computations decreases with the depth $z = (r_c - r)/R_\odot$ as $q \equiv (\partial \ln \Omega / \partial \ln r) \approx 3.1(x_c - z)u_{\max}$, where $x_c = r_c/R_\odot$, and $u_{\max} = \Delta\Omega(0, r_b)/10^{-6}$. In our basic parameter set, we will use a value of $u_{\max} = 10^{-4} \mu\text{Hz} \ll \Omega(r_c)$.

To solve eq. (5) one needs to know stellar structure parameters, such as ρ , N , K , and

others, as functions of radius and time. However, because the internal structure of the Sun has not changed appreciably in the last billion years, we will use our model of the present-day Sun as a background for all of our IGW computations and we will watch that the total integration time in each of them does not exceed ~ 1 Gyr. We have solved eq. (5) using an original method described in Appendix A.

5.1. Constant Viscosity

Fig. 4 shows our results obtained for different values of the constant viscosity $\nu_{0,n} \equiv \nu/10^n$ using the spectra (6) (panel a) and (7) (panel b). This figure illustrates the aforementioned bifurcation from stationary to oscillatory solutions that occurs at $\nu_{0,8} \approx 5 \times 10^{-4}$ in panel a and at $\nu_{0,8} \approx 8 \times 10^{-4}$ in panel b, a sequence of oscillatory solutions (these are analogs of the SLOs discussed by Talon & Charbonnel 2005) for $5 \times 10^{-5} \leq \nu_{0,8} \leq 5 \times 10^{-4}$ in panel a and for $7 \times 10^{-5} \leq \nu_{0,8} \leq 8 \times 10^{-4}$ in panel b, and a transition to the chaotic behavior of $\Delta\Omega$ at $\nu_{0,8} = 3.8 \times 10^{-5}$ in panel a and at $\nu_{0,8} = 4.9 \times 10^{-5}$ in panel b. Although in these computations we have only taken into account IGWs with frequencies from the narrower interval $0.3 \mu\text{Hz} \leq \omega \leq 0.6 \mu\text{Hz}$, this truncation does not depreciate our results because waves with these low frequencies carry 75% and 91% of the total energy for the spectral distributions (6) and (7), respectively. A comparison of panels a and b shows that the use of either of the two IGW spectra leads to similar qualitative results.

Since the low-frequency waves get absorbed very close to the core/envelope interface, we have taken the zooming parameter $k = 2.6$ (see Appendix A) in order to resolve the short lengthscale variations of the rotation profile produced by them. For this k and for the used value of $n = 8$, we get a time scaling factor of 9.7 yr for our dimensionless PDE (A3). The real timescales of the oscillations of $\Delta\Omega$ are somewhat longer than this because, additionally, they are inversely proportional to the amplitude of the second term on the right-hand side of the PDE which is of order $10^{-2} - 10^{-3}$. Therefore, the minimum time intervals between consecutive curves in Fig. 4 are 10^3 yr (panel a) and 10^2 yr (panel b). A decrease of ν_0 leads to both longer timescales and larger amplitudes of the oscillations because, in order to compete with the disturbing action of IGWs, a smaller viscosity needs a stronger shear to be built up, which means longer viscous dissipation times.

So far, we have used our basic parameter set that includes a limited number of $l = 1, 2, 3$, and 4, and uses $u_{\text{max}} = 10^{-4} \mu\text{Hz}$ in the initial and boundary conditions (9–10). Panel a in Fig. 5 demonstrates that neither the addition of 4 extra l values nor the increase of u_{max} by the factor 10^3 , which results in the initial shear $q \approx 0.22$ near the interface, change much the period and amplitude of the oscillations of $\Delta\Omega$.

Although the changes caused by the increase of $\Delta\Omega(0, r_b)$ (u_{\max}) turn out to be unimportant for our investigation of the ability of IGWs to disturb the internal uniform rotation of the present-day Sun, they were shown by Talon & Charbonnel (2005) to be a matter of great importance in the problem of angular momentum extraction by IGWs from the radiative core of a young solar-type MS star. Indeed, a steep initial $\Delta\Omega$ -profile results in the SLOs that are asymmetric with respect to the line $\Delta\Omega = 0$ (red curves in Fig. 5a). Such SLOs may work as a filter that predominantly absorbs prograde waves. This means that among low-degree high-frequency waves that arrive at a rapidly rotating central part of the star retrograde waves transporting negative angular momentum will be over-represented. Hence, when being damped in the core they will spin it down.

5.2. Shear-Induced Viscosity

The constant viscosity has been adjusted by hand to get one of the three possible outcomes of the competition between the disturbing action of IGWs and the smoothing effect of the viscous force on the rotation profile. It turns out that the quasi-periodic oscillations of $\Delta\Omega$ are settled only when ν_0 takes on a value from a rather narrow interval. It is unlikely that this accidentally happens in real stars. For the IGW filter composed of quasi-regular temporal and radial variations of $\Delta\Omega$ near the top of radiative core to work as proposed by Talon & Charbonnel (2005) some self-regulating mechanism for adjusting the proper viscosity values should apparently be operating there. One such mechanism could be a shear-induced viscous friction. In this case, a shear is readily built up as a result of selective damping of IGWs. Absorbed waves deposit their angular momentum locally, thus pushing rotation away from its stationary state. The viscosity coefficient (B2) used by us is appropriate for describing mixing due to the rotation-induced secular shear instability (Maeder & Meynet 1996). It develops more easily than the dynamical shear instability but it acts on a smaller length scale l_t , such that a turbulent eddy of size $\sim l_t$ can effectively exchange heat with its surroundings while it travels a mean free path of order $\sim l_t$.

Talon & Charbonnel (2005) have implemented this mechanism as follows. They averaged the turbulent diffusion coefficient (B6) over a complete oscillation cycle as well as over a radial extent of the SLOs using a Gaussian of width $0.2H_P$. Thus obtained stationary viscosity profile was then used in their IGW computations. As is said in Appendix B, we actually use the same viscosity (B2) but we allow it to vary with time and we do not average it over radius. For the same choice of IGW parameters as in the preceding section but for the shear-induced viscosity (B2) calculated with $f_v = 1$, results of our solution of the PDE (A3) with the spectrum (6) are plotted in Fig. 5b.

It is important to note that, like a few other publications (e.g., Kim & MacGregor 2001; Talon et al. 2002), the work of Talon & Charbonnel (2005) only contains a discussion of the SLOs near the core/envelope interface. Unlike them, we have decided to address the question whether the SLOs die out at greater depth or not. In order to shorten our computation time (i.e. in order to allow longer time steps) when solving the PDE (A3) in the bulk of radiative core we have bounded the IGW frequency by the values $0.6 \mu\text{Hz} \leq \omega \leq 3 \mu\text{Hz}$, i.e. we have cut off the IGWs that produce the SLOs very close to the interface, like those shown in Fig. 5b. In spite of this, our minimum frequency still approximately equals the lowest frequency $0.5 \mu\text{Hz}$ used by Charbonnel & Talon (2005). It is important to note that the IGW spectra we use are still normalized by equation (2) over the whole frequency and spherical degree intervals: $0.3 \mu\text{Hz} \leq \omega \leq 3 \mu\text{Hz}$, and $1 \leq l \leq l_c = 30$. Because of its rapid decline with an increase of ω a spectrum normalized with $\omega_{\min} > 0.3 \mu\text{Hz}$ would have more energetic high-frequency waves than ours, hence it would produce even stronger oscillations of $\Delta\Omega$ than those obtained by us.

We have solved equation (A3) in the $k=1$ -zoomed depth interval $0 \leq \hat{z} \leq \hat{z}_b = 10^k \times (x_c - x_b)$, where $x_c = 0.713$ and $x_b = x_c - 0.6$, for time periods less than 1 Gyr. Hoping to relate, later on, the angular momentum transport and element mixing by IGWs in the Sun to canonical extra mixing in low-mass red giants, we have taken the parameter $f_v = 20$ in the expression (B2) for the shear-induced viscosity because with about that value Denissenkov et al. (2006) succeeded in reproducing evolutionary abundance variations of Li and C in the atmospheres of cluster and field red giants. We have found that, even after having been enhanced by this large factor, the shear-induced viscosity fails to extinguish large scale SLOs deeper in the solar radiative core. The blue curve in Fig. 6a represents an envelope of oscillation amplitudes of $\Delta\Omega$. The farther inward from the core/envelope interface, the higher the $\Delta\Omega$ oscillation amplitude and the longer its characteristic time are. In the outer half of the radiative core the maximum amplitudes by far exceed the deviations of the helioseismic data (red squares with error bars) from the uniform rotation profile. A better agreement with the experimental data is obtained if we choose $f_v = 10^3$ (purple curve in panel a). We have tried this value as well because the 3D hydrodynamic simulations by Brüggén & Hillebrandt (2001) of turbulent mixing induced by the shear instability have shown that equation (B1) may underestimate the coefficient of turbulent diffusion by three orders of magnitude. Of course, it is not clear whether the results of Brüggén & Hillebrandt (2001) can be applied directly to real stars, given that they were obtained assuming plane-parallel geometry and without taking into account “the effects of rotation, nuclear reactions, and variations in radiative processes”.

However, before making any conclusions from the results of these computations we have to check if the viscosities induced by the shear flows outlined in panel a are high enough for

the turbulent fluid motions producing them not to be broken down by the molecular viscosity. For this to be true, the flow Reynolds number $Re = \nu_v / \nu_{\text{mol}}$ must exceed the critical Reynolds number $Re_c \approx 40$ (Schatzman et al. 2000). In panel b, we have plotted a time averaged ν_v for the cases of $f_v = 20$ (blue curve) and $f_v = 10^3$ (purple curve). In the same plot, green curve depicts ν_{mol} while red curve presents the quantity $Re_c \times \nu_{\text{mol}}$. Comparing blue, purple, and red curves in panel b, we conclude that the shear-induced turbulence can only be sustained near the base of the convection zone where both the shear q is sufficiently strong thanks to the very short lengthscales of the SLOs and the quantity proportional to $\nu_v f_v^{-1} (\Omega q)^{-2}$ (eq. B1 and dashed curve in Fig. 3) steeply increases with r . This raises the following important question: what alternative shear dissipating mechanism works in the Sun’s outer radiative core that successfully competes (as follows from the helioseismic data) with the disturbing action of IGWs?

5.3. Molecular Viscosity and Ohmic Diffusivity

Fig. 6 shows that the viscosity needed to counteract the distortion of the solar rotation profile by IGWs should not necessarily be too high. Taking into account that the blue and purple curves in Fig. 6b represent the time averaged ν_v , whose real values change with time following the oscillations of $\Delta\Omega$, it seems worth testing if the molecular viscosity can smooth out the large scale SLOs alone. The shear-induced turbulent viscosity can only be used down to a depth $z \approx 0.04 - 0.05$ because below this region the ratio ν_v / ν_{mol} becomes smaller than the critical Reynolds number (Fig. 6b). It is interesting that the size of this region approximately coincides with the thickness of the solar tachocline in which the latitudinal differential rotation of the convective envelope is transformed into the quasi-solid body rotation of the radiative core (e.g., Spiegel & Zahn 1992; Charbonneau et al. 1998). We want to find out if the viscous force in our computations fails to reduce amplitudes of the SLOs in the outer radiative core to values consistent with the helioseismic data simply because we use the IGW spectrum (6) instead of (7).

It is possible that this negative result is a function of the assumed IGW spectrum. In order to respond to these questions, we have employed the spectrum (7) and a combined viscosity $\nu = \nu_v(f_v) + f_{\text{mol}} \times \nu_{\text{mol}}$, where $\nu_v(f_v)$ is a substitute of equation (B2) in which we set $f_v = 20$ for $0 \leq z \leq 0.04$ and $f_v = 0$ for $0.04 < z \leq z_b$. We have also investigated models with more vigorous IGWs. Furthermore, as Charbonnel & Talon (2005) claimed, the total energy luminosity of IGWs produced by fluctuating Reynolds stresses in the convective envelope of their solar model was $8.5 \times 10^{29} \text{ erg s}^{-1}$. This is about 2.7 times as large as our estimated value of $L_E(r_c) \approx 3.2 \times 10^{29} \text{ erg s}^{-1}$. Therefore, we have increased our turbulent Mach number

$\mathcal{M}_t = 8.3 \times 10^{-4}$ by this factor and renormalized the spectrum (7) respectively. Results of these computations obtained with the factor $f_{\text{mol}} = 2$ are plotted with purple curves in Fig. 7. For test purposes, we have also repeated these computations with an extended set of the spherical degree $l = 1, 2, \dots, 7, 8$ (blue curves). Fig. 7 shows that the molecular viscosity (even after it has been doubled) cannot compete with the IGWs that have been shown by Charbonnel & Talon (2005) to be powerful enough to shape the Sun’s solid body rotation.

On the other hand, it turns out that a viscosity proportional to the ohmic diffusivity $\nu = f_{\text{mag}} \times \eta_{\text{mag}}$ can extinguish the IGW-induced SLOs everywhere in the solar radiative core except the tachocline region for a value of $f_{\text{mag}} \gtrsim 10$ (Fig. 8). This seemingly pure academic exercise has some sense. Let us assume that differential rotation in the solar radiative core has been suppressed by magnetic processes, e.g. like those proposed by Charbonneau & MacGregor (1993), Menou & Le Mer (2006), or Spruit (1999) (for more details on the latter, see next section). However, in order that magnetic fields generated by these processes not to decay too quickly through the ohmic dissipation, an effective magnetic diffusivity η_e associated with them must exceed η_{mag} .

5.4. Effective Magnetic Viscosity

Spruit (1999) has proposed a magnetohydrodynamic mode of angular momentum transport in radiative zones of differentially rotating stars. Fluid elements experience large-scale horizontal displacements caused by an unstable configuration of the toroidal magnetic field (one consisting of stacks of loops concentric with the rotation axis). Small-scale vertical displacements of fluid elements are coupled to the horizontal motions, which can cause both mild mixing and much more effective angular momentum transport. Spruit’s key idea is that no initial toroidal magnetic field is actually needed to drive the instability and mixing because the unstable field configuration can be generated and maintained by differential rotation in a process similar to convective dynamo. The Spruit dynamo cycle consists of two consecutive steps: first, a poloidal field is generated by the vertical displacements of the unstable toroidal field; second, the new poloidal field is stretched into a toroidal field by differential rotation.

The Spruit mechanism produces a huge magnetic viscosity $\nu_e \gtrsim 10^9 \text{ cm}^2 \text{ s}^{-1}$ (Denissenkov & Pinsonneault 2007) that could indeed prevent IGWs from disturbing the solar uniform rotation. However, it could produce that uniform rotation itself, without being assisted by IGWs (Eggenberger et al. 2005).

The original prescription for the effective magnetic diffusivity and viscosity in the model

of Spruit’s dynamo has recently been criticized by Denissenkov & Pinsonneault (2007) (see also Zahn et al. 2007). The principal critical argument is that Spruit (1999) has overestimated the horizontal length scale of the Tayler instability that causes the concentric magnetic loops to slip sideways. Spruit assumed the length was of order a local stellar radius. Denissenkov & Pinsonneault (2007) suggested that one has to account of the Coriolis force when estimating the instability’s horizontal length scale. This reduces the diffusivity by about three orders of magnitude and results in the following expression:

$$\eta_e \approx 2 \frac{K_6 \Omega_{-6}^2}{(N_T)_{-3}^2} q^2, \quad \text{cm}^2 \text{s}^{-1}. \quad (11)$$

There is no need to do any further computations to understand that, with this revised diffusivity, magnetic fields generated by the Spruit dynamo in the solar radiative core would immediately be dissipated through the ohmic diffusivity, hence the whole transport mechanism would not function. Indeed, equation (11) gives $\eta_e \approx 1.8 \times 10^2 \text{ cm}^2 \text{ s}^{-1} < \eta_{\text{mag}}$ near the base of the solar convection zone even if we take $q \approx 1$ which obviously exceeds the upper limit constrained by the helioseismic data. The revised prescription may only work to reduce differential rotation in a model of the young Sun in which both Ω_{-6} and q have much larger values (Denissenkov et al., in preparation).

6. Conclusion

Our numerical solutions of the angular momentum transport equation (5, or A3) have demonstrated that neither the molecular viscosity nor the shear-induced turbulent viscosity can reduce the large scale oscillations of angular velocity in the solar outer radiative core caused by selective damping of IGWs, provided that the net energy flux of these waves is strong enough to shape the Sun’s solid body rotation. If waves were the sole mechanism, we would therefore expect to see large deviations from rigid rotation. The amplitudes of these oscillations are found to be too large to agree with the helioseismic data. Our result holds even when the molecular and shear-induced viscosity are multiplied by large factors. We have proved that only a viscosity exceeding the ohmic diffusivity by a factor of $\gtrsim 10$ can smooth out the IGW-induced oscillations of the rotation profile. This may be an indirect indication that some magnetic processes are at work here. To be more precise, our finding actually satisfies a necessary condition for such processes to work because the effective magnetic diffusivity η_e associated with them must exceed the ohmic diffusivity η_{mag} . Otherwise magnetic fields generated by them will decay through the ohmic resistivity too quickly. For example, we have found that magnetic torques are strong enough to successfully compete with the action of IGWs only if the original prescription for the Taylor-Spruit dynamo, in which $\eta_e \gg \eta_{\text{mag}}$,

is used. However, this particular case turns out to be irrelevant to our problem because the Tayler-Spruit mechanism can shape the solar solid body rotation alone (Eggenberger et al. 2005), without being assisted by IGWs.

The helioseismic data suggest that either there is an efficient angular momentum transport mechanism in addition to IGWs that smooths out the SLOs produced by the waves or the spectral energy distribution of IGWs is different (lower) from those used by us. Although the latter assumption leads us outside the scope of our formulated problem we will comment on it. It is possible that strong toroidal magnetic fields in the solar tachocline filter out the IGWs with the doppler-shifted frequency σ above the Alfvén frequency (Kumar et al. 1999; Kim & MacGregor 2003). For the minimum frequency $0.6 \mu\text{Hz}$ used in our computations of the large scale SLOs in the solar outer radiative core the magnetic field strength required to prevent the inward wave propagation is about $(3 \times 10^5)/l$ Gauss (Kumar et al. 1999). For $l = 1$, this corresponds to quite a strong field. If it is present in the tachocline then the waves with high spherical degrees will be trapped there. However, we have only considered IGWs with $\omega \geq 0.6 \mu\text{Hz}$ and low l values. Most of them are likely to propagate below the tachocline. In order to find out if an enhanced viscosity in the tachocline can hinder the propagation of low-degree high-frequency waves into the solar radiative core we have done test computations in which the shear-induced viscosity was increased by a factor of 10^3 . Their results plotted with black curves in Fig. 7 show that this does not help to solve the problem.

Another, more radical possibility is that the form of the IGW spectra employed by us is completely wrong. For instance, the IGW spectrum estimated in the 2D hydrodynamic simulations by Rogers & Glatzmaier (2005) has a flat energy distribution which goes three orders of magnitude below the peak luminosity in our Fig. 1. Apparently, if we applied that spectrum in our computations then even the molecular viscosity could easily smooth out the SLOs produced by such IGWs. However, it is evident as well that IGWs with this energy distribution could not produce the uniform rotation of the Sun by its present age (multiply the ages of the rotation profiles in Fig. 1 from Charbonnel & Talon 2005 by a thousand).

To summarize, we do not see what microscopic or pure hydrodynamic processes could smooth out the large scale SLOs induced by IGWs in the solar outer radiative core. Therefore, we agree with the conclusion made by Gough & McIntyre (1998) about “the inevitability of a magnetic field in the Sun’s radiative interior”. Indeed, if IGWs are as strong as described by our employed spectra then this magnetic field is required to trigger magnetic processes that will counteract the disturbing action of IGWs on the solar rotation profile. On the contrary, if IGWs are weak then we are in need of such magnetic processes to extract an excess angular momentum from the solar interior on the early MS.

During the preparation of this work, results of a preliminary analysis of the GOLF data on solar g-mode oscillations have been published by García et al. (2007) suggesting that the solar core at $r \lesssim 0.15 R_\odot$ may rotate three to five times as fast as the rest of the radiative core. If these results prove to be correct, they will seem to rule out the angular momentum redistribution in the Sun by IGWs, as proposed by Charbonnel & Talon (2005), because in that case it would have been the Sun’s inner core to be spun down first. If these results are confirmed, it will mean that the strong μ -gradient in the Sun’s central region has prevented any angular momentum transport mechanism from operating there. There would also be strong implications for magnetic angular momentum transport, ruling out prescriptions (such as Spruit 2002) that predict a weak sensitivity to μ gradients.

We acknowledge support from the NASA grant NNG05 GG20G. PAD thanks Tamara Rogers for useful discussions and the HAO staff for the warm hospitality. The National Center for Atmospheric Research is sponsored by the National Science Foundation.

A. Solution of the Angular Momentum Transport Equation

In order to shrink the problem’s parameter space, we consider a contribution to the transport of angular momentum only from the waves possessing the maximum possible azimuthal number $|m| = l$, i.e. from those carrying the maximum angular momentum, both positive and negative, at given values of l and ω . To solve the main PDE (5), we use a numerical method based on the ideas implemented by Saravanan (1990) in his model of the wind flow in the Earth’s stratosphere influenced by tropospheric IGWs.

Taking into account the assumed axial symmetry of the IGW spectrum, i.e. that $S_E(r_c, l, m, \omega) = S_E(r_c, l, -m, \omega)$, and the fact that the optical depth in the wave attenuation factor only depends on even powers of the doppler-shifted frequency σ (eq. 1), we recast the net angular momentum flux for $m = \pm l$ as

$$F_J(r) \equiv \frac{L_J(r)}{4\pi r_c^2} = \sum_{l=1}^{l_{\max}} l \int_{-\omega_{\max}}^{\omega_{\max}} S_J(l, \omega) \exp\{-\tau(r, l, l, \omega)\} d\omega, \quad (\text{A1})$$

where

$$S_J(l, \omega) \equiv S_E(r_c, l, l, |\omega|) \omega^{-1}. \quad (\text{A2})$$

In the interval $-\omega_c < \omega < \omega_c$, we set $S_J(l, \omega) \equiv 0$. Note that $S_J(l, -\omega) = -S_J(l, \omega)$.

From the computational standpoint, we find it convenient to convert eq. (5) to the following dimensionless form:

$$\frac{\partial u}{\partial \hat{t}} = \frac{1}{\rho x^4} \frac{\partial}{\partial \hat{z}} \left(\rho x^4 \nu_n \frac{\partial u}{\partial \hat{z}} \right) - \frac{a_{n,k}}{\rho x^4} \left(\frac{L}{L_\odot} \right) \frac{\partial F}{\partial \hat{z}}, \quad (\text{A3})$$

where $x = r/R_\odot$, and

$$F(\hat{z}, u) = \frac{10^3}{\rho_c v_c^3} \sum_{l=1}^{l_{\max}} l \int_{-\omega_{\max}}^{\omega_{\max}} S_J(l, \omega) \exp\left\{-\int_0^{\hat{z}} G(\hat{z}', l, \omega - lu) d\hat{z}'\right\} d\omega. \quad (\text{A4})$$

In the last equation, $G(\hat{z}, l, \omega - lu) = [l(l+1)]^{3/2} \gamma^{-1}(\hat{z}) (\omega - lu)^{-4}$, where $\gamma^{-1}(\hat{z}) = 10^{-k} \times 0.2065 \times K_6 N_{-3} (N_T)_{-3}^2 (x_c - 10^{-k} \hat{z})^{-3}$ with $x_c = r_c/R_\odot$. We neglect the square root $\sqrt{1 - (\sigma/N)^2}$ in the integrand's denominator in eq. (1) because we will only consider $\omega_{\max} \ll N_c$ in which case $|\sigma| \equiv |\omega - lu| < 2\omega_{\max} \ll N$.

When deriving eqs. (A3–A4), we have normalized our basic variables, which are assumed to be initially expressed in cgs units, as follows: $u = \Delta\Omega/10^{-6}$, $\nu_n = \nu/10^n$, $\hat{z} = 10^k \times (x_c - x)$, $\hat{t} = (10^{n+2k}/R_\odot^2) t$, $K_6 = K/10^6$, and $N_{-3} = N/10^{-3}$. The quantity k is a sort of zooming parameter. Taking $k > 0$ allows us to look with the scrutiny at results of IGW damping taking place close to the base of convective envelope, where variations of u may occur on a very short lengthscale of order $10^{-3} - 10^{-2} R_\odot$. Having done these transformations, it turns out that $a_{n,k} = 1.362 \times 10^{8-n-k}$, $\hat{z} = 0$ corresponds to the core/envelope interface, and t is measured in units of $1.535 \times 10^{14-n-2k}$ yr. The factor 10^3 in eq. (A4) comes about from a combination of the factor 0.1 that estimates the ratio of the convective flux to the total flux from the star and the factor 10^4 that represents the reciprocal to the normalization constant for the turbulent Mach number that has been included into the coefficient $a_{n,k}$. Given that ω is measured in μHz , $a_{n,k}$ has additionally been multiplied by the factor 10^6 . This is necessary to do because the wave frequency that we actually use is $\omega \equiv \omega/10^{-6}$, therefore, when substituted into eq. (A4), relation (A2) should be taken in the form $S_J = 10^6 \times S_E (\omega/10^{-6})^{-1}$.

In equations (A3–A4), all integrals are replaced with series of trapezoids while all derivatives are approximated by finite differences. The zoomed depth interval $0 \leq \hat{z} \leq \hat{z}_b$ (here, $\hat{z}_b = 10^k (r_c - r_b)/R_\odot$) is divided into M equal subintervals by $M+1$ mesh points while the axisymmetric frequency intervals $-\omega_{\max} \leq \omega \leq -\omega_c$ and $\omega_c \leq \omega \leq \omega_{\max}$, representing the retrograde and prograde waves, respectively, are divided into L subintervals each. The resulting system of $M+1$ nonlinear algebraic equations is linearized assuming that after every integration time step $\Delta \hat{t}$ the ratio $\max\{|\Delta u_j/u_j|\}_{j=2}^M \ll 1$. In order to speed up the computations, we follow the idea of Saravanan (1990) to interpolate functions containing

$G(\hat{z}_j, l, \omega_i - lu_j)$ in \hat{z}_j, l , and the combination $(\omega_i - lu_j)$ using initially prepared and stored tables.²

B. Viscosity Prescriptions

The viscosity ν in eq. (5) plays a very important role because, depending on its value, the viscous friction either succeeds or not in smoothing out oscillations of the rotation profile in the radiative core growing in response to the local deposit of angular momentum that accompanies the absorption of IGWs. In this work, we employ 5 different prescriptions for ν as well as some of their combinations. These are a constant viscosity ν_0 , the molecular viscosity ν_{mol} (it dominates over the radiative viscosity in the solar-type MS stars), a viscosity proportional to the magnetic (ohmic) diffusivity η_{mag} , a viscosity ν_v associated with vertical turbulence produced by the secular shear instability induced by differential rotation, and an effective viscosity ν_e related to magnetic torques generated by the Tayler-Spruit dynamo (Spruit 1999, 2002).

For the viscosity due to the shear-induced vertical turbulence, we use the expression derived by Maeder & Meynet (1996) multiplying it by a free parameter f_v

$$\nu_v = f_v \times \frac{8}{5} Ri_c \frac{K}{N_T^2} \Omega^2 q^2, \quad (\text{B1})$$

where $Ri_c = \frac{1}{4}$ is the critical Richardson number, and the shear $q = (\partial \ln \Omega / \partial \ln r)$. The parameter f_v takes into account the fact that, according to hydrodynamic simulations by Brüggén & Hillebrandt (2001), the original prescription may underestimate the viscosity by the factor of $\sim 10^3$. Alternatively, Canuto (2002) has supposed that Ri_c should be at least four times as large as its classical value. After the same normalization used in Appendix A, we have

$$(\nu_v)_n = f_v \times \frac{2}{5} 10^{2k-n} x^2 \frac{K_6}{(N_T)_{-3}^2} \left(\frac{\partial u}{\partial \hat{z}} \right)^2. \quad (\text{B2})$$

To compute the effective magnetic viscosity, we use both original Spruit's equations (see our §5.4) and the equations revised by Denissenkov & Pinsonneault (2007)

$$\nu_e = \left(\frac{r^2 \Omega \eta_e^2}{q^2} \right)^{1/3}, \quad (\text{B3})$$

²We take advantage of the fact that $|\omega_i - lu_j| < 2\omega_{\text{max}}$.

where the effective magnetic diffusivity is

$$\eta_e \approx 2 \frac{K}{N_T^2} \Omega^2 q^2. \quad (\text{B4})$$

Combining the last two equations and normalizing the variables, we find

$$(\nu_e)_n = 2.686 \times 10^5 \times 10^{\frac{2}{3}k-n} \Omega_{-6} \left[x^2 \frac{K_6}{(N_T)_{-3}^2} \right]^{2/3} \left(\frac{\partial u}{\partial \hat{z}} \right)^{2/3}. \quad (\text{B5})$$

It should be noted that we have implicitly assumed that $N_\mu^2 = 0$ in eqs. (B1) and (B4). This approximation may be valid in the outer part of radiative core if we neglect the μ -gradients produced by the gravitational settling and radiative levitation of chemical elements. Under this assumption, our choice of ν_v is equivalent to that made by Talon & Charbonnel (2005). Indeed, although they have used a prescription proposed by Talon & Zahn (1997)

$$\tilde{\nu}_v = \frac{8}{5} Ric \frac{K}{N_T^2} \Omega^2 q^2 \frac{(1 + D_h/K)}{1 + (N_\mu^2/N_T^2)(1 + K/D_h)} \quad (\text{B6})$$

that takes into account a reduction of the stable thermal stratification in the radiative core by strong horizontal turbulence described with a diffusion coefficient $D_h \gg \tilde{\nu}_v$, putting $N_\mu^2 = 0$ in eq. (B6) and noticing that in evolved solar-type MS stars $D_h \ll K$ (e.g., see Fig. 14 in the paper of Talon & Charbonnel 2005) transforms $\tilde{\nu}_v$ into our ν_v .

REFERENCES

- Barnes, S. A. 2003, *ApJ*, 586, 464
- Bouvier, J., Forestini, M., & Allain, S. 1997, *A&A*, 326, 1023
- Brüggen, M., & Hillebrandt, W. 2001, *MNRAS*, 320, 73
- Canuto, V. M. 2002, *A&A*, 384, 1119
- Cattaneo, F., Brummell, N. H., Toomre, J., Malagoli, A., & Hurlburt, N. E., 1991, *ApJ*, 370, 282
- Charbonneau, P., & MacGregor, K. B. 1993, *ApJ*, 417, 762
- Charbonneau, P., Tomczyk, S., Schou, J., & Thompson, M. J. 1998, *ApJ*, 496, 1015
- Charbonnel, C., & Talon, S. 2005, *Science*, 309, 2189

- Couvidat, S., García, R. A., Turck-Chièze, Corbard, T., Henney, C. J., & Jiménez-Reyes, S. 2003, *ApJ*, 597, L77
- Denissenkov, P. A., & Vandenberg, D. A. 2003, *ApJ*, 593, 509
- Denissenkov, P. A., Chaboyer, B., & Li, K. 2006, *ApJ*, 641, 1087
- Denissenkov, P. A., & Pinsonneault, M. 2007, *ApJ*, 655, 1157
- Eggenberger, P., Maeder, A., & Meynet, G. 2005, *A&A*, 440, L9
- García López, R. J., & Spruit, H. C. 1991, *ApJ*, 377, 268
- García, R. A., Turck-Chièze, S., Jiménez-Reyes, S. J., Ballot, J., Pallé, P. L., Eff-Darwich, A., Mathur, S., & Provost, J. 2007, *Science*, 316, 1591
- Goldreich, P., Murray, N., & Kumar, P. 1994, *ApJ*, 424, 466
- Gough, D., & McIntyre, M. E. 1998, *Nature*, 394, 755
- Grevesse, N., & Noels, A. 1993, in *Origin and Evolution of the Elements*, ed.. N. Prantzos, E. Vangioni-Flam, & M. Casse (Cambridge: Cambridge Univ. Press), 15
- Kawaler, S. D. 1988, *ApJ*, 333, 236
- Keppens, R., MacGregor, K. B., & Charbonneau, P. 1995, *A&A*, 294, 469
- Kim, E.-J., & MacGregor, K. B. 2001, *ApJ*, 556, L117
- Kim, E.-J., & MacGregor, K. B. 2003, *ApJ*, 588, 645
- Kiraga, M., Stepien, K., & Jahn, K. 2005, *AcA*, 55, 205
- Krishnamurthi, A., Pinsonneault, M. H., Barnes, S., & Sofia, S. 1997, *ApJ*, 480, 303
- Kumar, P., & Quataert, E. J. 1997, *ApJ*, 475, L143
- Kumar, P., Talon, S., & Zahn, J.-P. 1999, *ApJ*, 520, 859
- Lighthill, J. 1978, *Waves in Fluids*, (Cambridge: Cambridge Univ. Press), Chap. 5
- Lindzen, R. S., & Holton, J. R. 1968, *J. Atmos. Sci.*, 25, 1095
- Maeder, A., & Meynet, G. 1996, *A&A*, 313, 140
- Matt, S., & Pudritz, R. E. 2008, arXiv:0801.0436v2 [astro-ph]

- Menou, K., & Le Mer, J. 2006, *ApJ*, 650, 1208
- Montalbán, J., & Schatzman, E. 2000, *A&A*, 354, 943
- Plumb, R. A. 1977, *J. Atmos. Sci.*, 34, 1847
- Press, W. H. 1981, *ApJ*, 245, 286
- Rieutord, M., & Zahn, J.-P. 1995, *A&A*, 296, 127
- Ringot, O. 1998, *A&A*, 335, L89
- Rogers, T. M., & Glatzmaier, G. A. 2005, *MNRAS*, 364, 1135
- Rogers, T. M., & Glatzmaier, G. A. 2006, *ApJ*, 653, 756
- Saravanan, R. 1990, *J. Atmos. Sci.*, 47, 2465
- Schatzman, E., Zahn, J.-P., & Morel, P. 2000, *A&A*, 364, 876
- Sestito, P., & Randich, S. 2005, *A&A*, 442, 615
- Sills, A., & Pinsonneault, M. H. 2000, *ApJ*, 540, 489
- Spiegel, E. A., & Zahn, J.-P. 1992, *A&A*, 265, 106
- Spruit, H. C. 1999, *A&A*, 349, 189
- Spruit, H. C. 2002, *A&A*, 381, 923
- Stauffer, J. R., & Hartmann, L. W. 1987, *ApJ*, 318, 337
- Stein, R. F., & Nordlund, A. 1989, *ApJ*, 342, L95
- Talon, S., & Zahn, J.-P. 1997, *A&A*, 317, 749
- Talon, S., Kumar, P., & Zahn, J.-P. 2002, *ApJ*, 574, L175
- Talon, S., & Charbonnel, C. 2003, *A&A*, 405, 1025
- Talon, S., & Charbonnel, C. 2005, *A&A*, 440, 981
- Yoden, S., & Holton, J. R. 1988, *J. Atmos. Sci.*, 45, 2703
- Zahn, J.-P., Talon, S., & Matias, J. 1997, *A&A*, 322, 320
- Zahn, J.-P., Brun, A. S., & Mathis, S. 2007, *A&A*, 474, 145

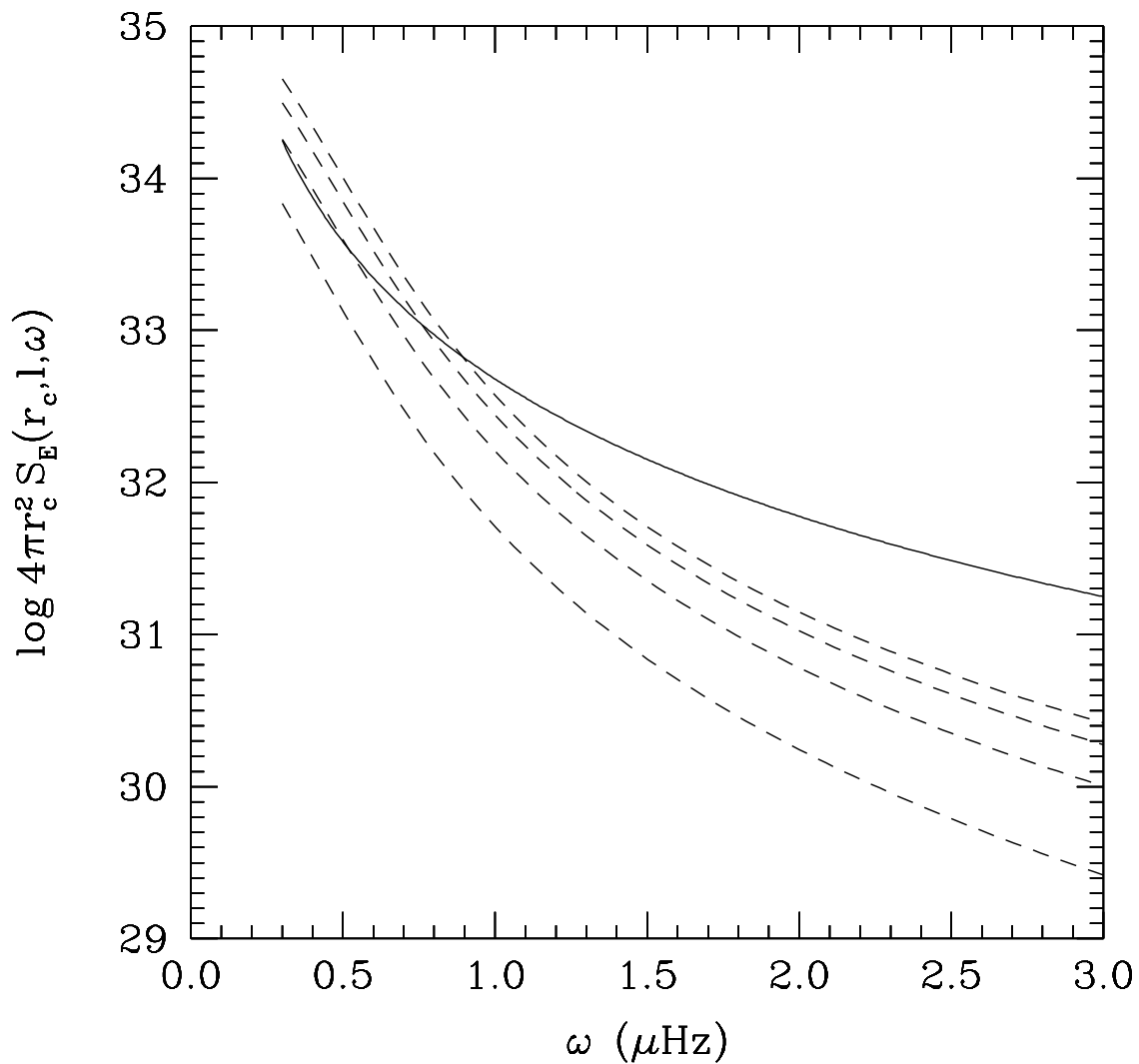


Fig. 1.— Logarithms of the energy luminosity of IGWs at the Sun’s core/envelope interface summed over all available azimuthal numbers ($m = -l, \dots, l$) as functions of l and ω . Solid curve corresponds to spectrum (6), dashed curves — to spectrum (7) for $l = 1, 2, 3$, and 4 (from the lower to upper curve).

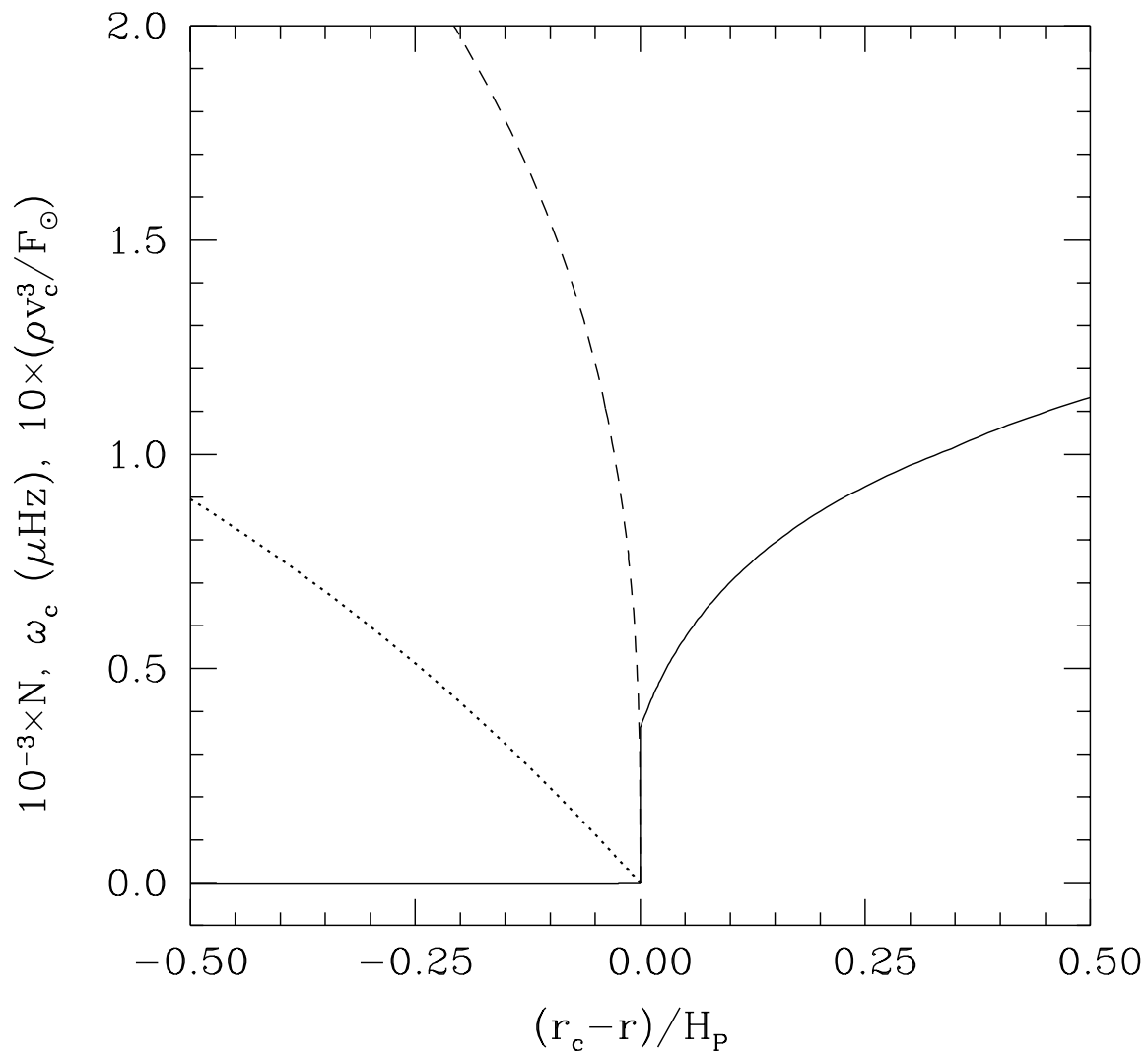


Fig. 2.— The convective overturn frequency ω_c (dashed curve), the buoyancy frequency N (solid curve), and the ratio of the convective flux ρv_c^3 to the total flux F_\odot (dotted curve) as functions of the relative depth (expressed in units of the pressure scale height) on the both sides of the Sun’s core/envelope interface.

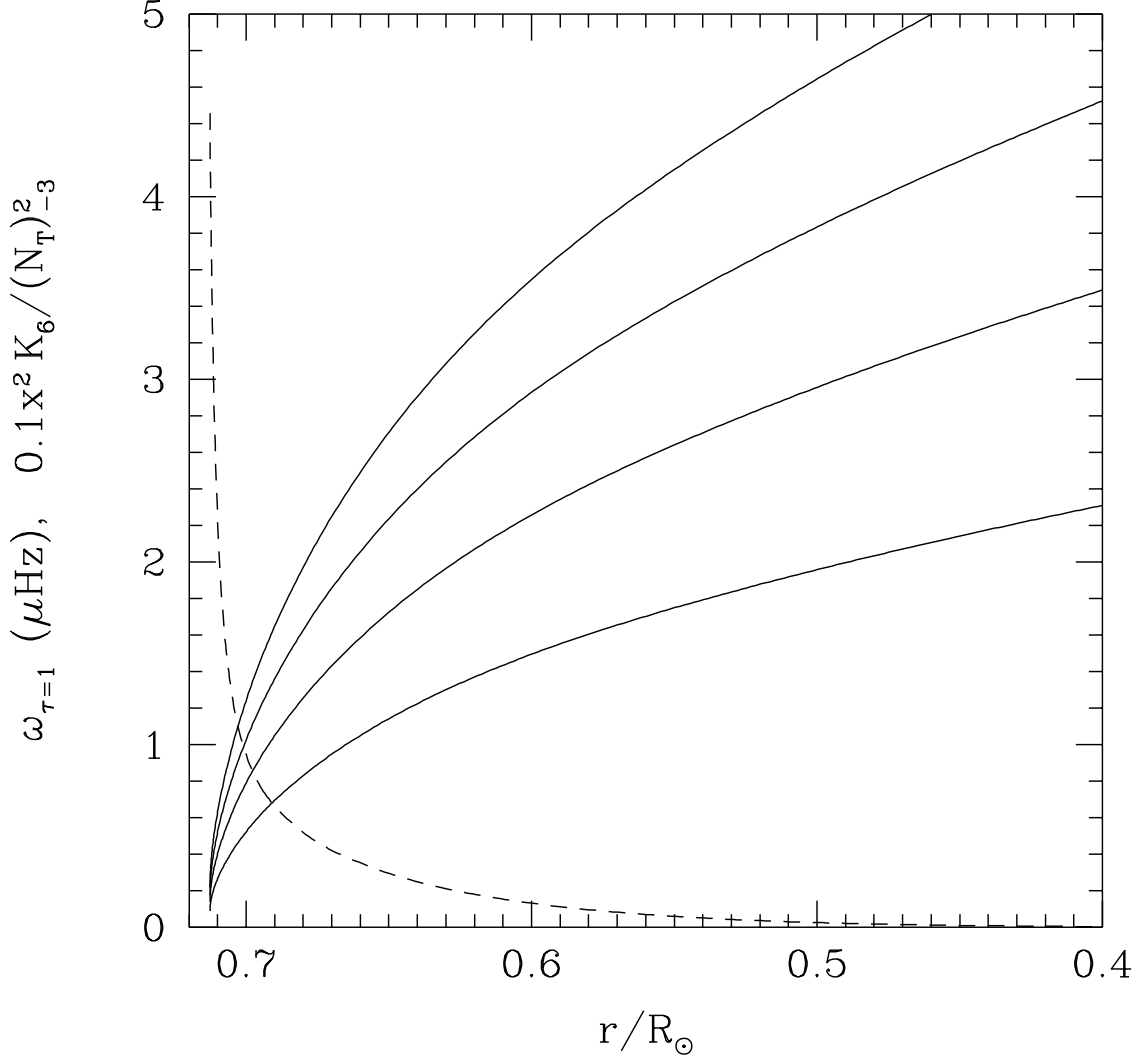


Fig. 3.— The frequency $\omega_{\tau=1}$ for which the effective optical depth (eq. 1) in the IGW attenuation factor $\exp(-\tau)$ equals to one at a given radius in the case of uniform rotation (from the lower to upper solid curve: l increases from 1 to 4, and $\omega_{\tau=1} \propto [l(l+1)]^{3/8}$). Dashed curve is the normalized stellar structure parameter in expression (B1) for the shear-induced viscosity.

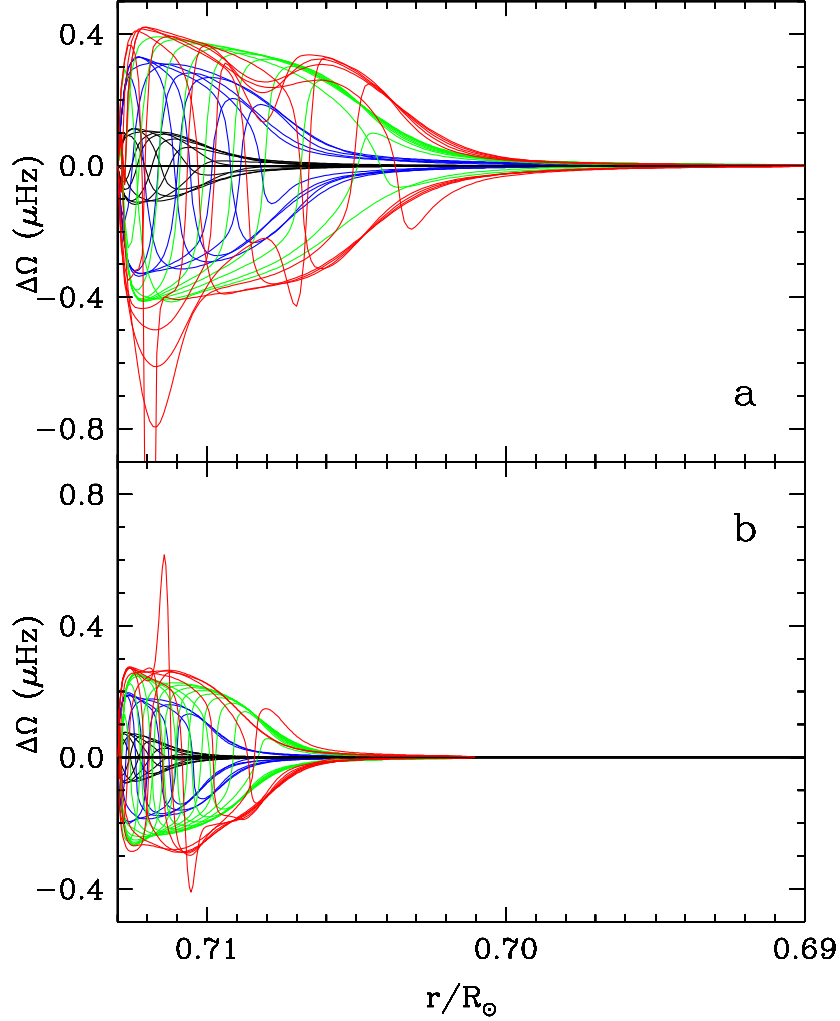


Fig. 4.— The shear-layer oscillations (SLOs) of $\Delta\Omega = \Omega(r) - \Omega_c$ at the top of solar radiative core computed (eq. A3) with the constant viscosity $\nu_{0,8} \equiv \nu_0/10^8$ using the IGW spectra (6) (panel a) and (7) (panel b) for the following sets of parameters: $0.3 \mu\text{Hz} \leq \omega \leq 0.6 \mu\text{Hz}$; $l = 1, 2, 3, 4$; $m = \pm l$; and $u_{\text{max}} = 10^{-4} \mu\text{Hz}$ in the boundary and initial conditions (9–10). Panel a: black curves — $\nu_{0,8} = 5 \times 10^{-4}$, the time interval between consecutive curves is $\Delta t = 10^3$ yr; blue — $\nu_{0,8} = 10^{-4}$, $\Delta t = 5 \times 10^3$ yr; green — $\nu_{0,8} = 5 \times 10^{-5}$, $\Delta t = 5 \times 10^3$ yr; red — $\nu_{0,8} = 3.8 \times 10^{-5}$, $\Delta t = 10^4$ yr. Panel b: black — $\nu_{0,8} = 8 \times 10^{-4}$, $\Delta t = 10^2$ yr; blue — $\nu_{0,8} = 10^{-4}$, $\Delta t = 10^3$ yr; green — $\nu_{0,8} = 7 \times 10^{-5}$, $\Delta t = 10^3$ yr; red — $\nu_{0,8} = 4.9 \times 10^{-5}$, $\Delta t = 2 \times 10^3$ yr.

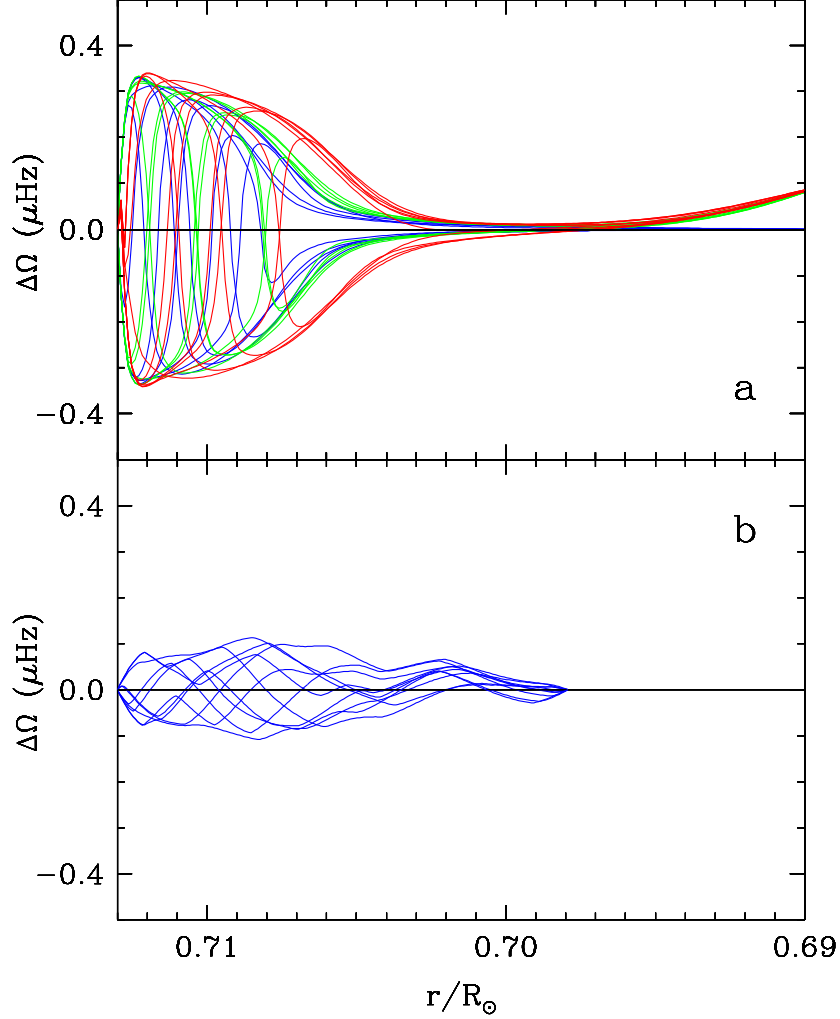


Fig. 5.— The SLOs at the top of solar radiative core computed with the constant (panel a) and shear-induced (panel b) viscosity using the IGW spectrum (6) and the same sets of basic parameters as in the previous figure. Exceptions are the enhanced value of $u_{\max} = 0.1 \mu\text{Hz}$ for green and red curves, and the extended set of $l = 1, 2, \dots, 7, 8$ for red curve. In panel a, all curves have $\nu_{0,8} = 10^{-4}$, and $\Delta t = 5 \times 10^3$ yr. Curves in panel b have been computed using the parameter $f_v = 1$ in eq. (B2), and $\Delta t = 5 \times 10^3$ yr.

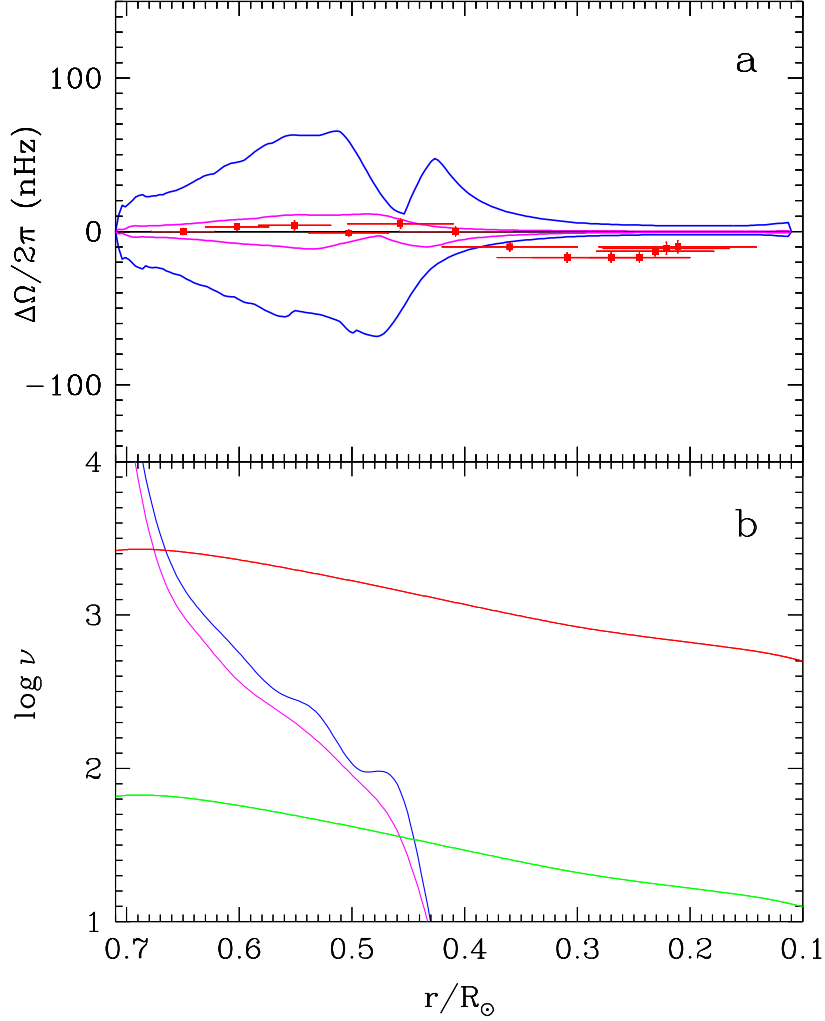


Fig. 6.— Panel a: blue and purple curves are the envelopes of amplitudes of the SLOs deep in the solar radiative core computed with the shear-induced viscosity (eq. B2 with $f_v = 20$ — blue curve, and with $f_v = 10^3$ — purple curve) using the IGW spectrum (6) and the same sets of basic parameters as in Fig. 4, except for the cut-off frequency interval $0.6 \mu\text{Hz} \leq \omega \leq 3 \mu\text{Hz}$. Red squares with error bars in panel a are the helioseismic data from Couvidat et al. (2003). Panel b: green curve — the molecular viscosity ν_{mol} ; red — the quantity $Re_c \times \nu_{\text{mol}}$, where the critical Reynolds number $Re_c = 40$ (Schatzman et al. 2000); blue and purple curves — the time averaged shear-induced viscosities produced by the SLOs whose envelopes are plotted in panel a with the same color.

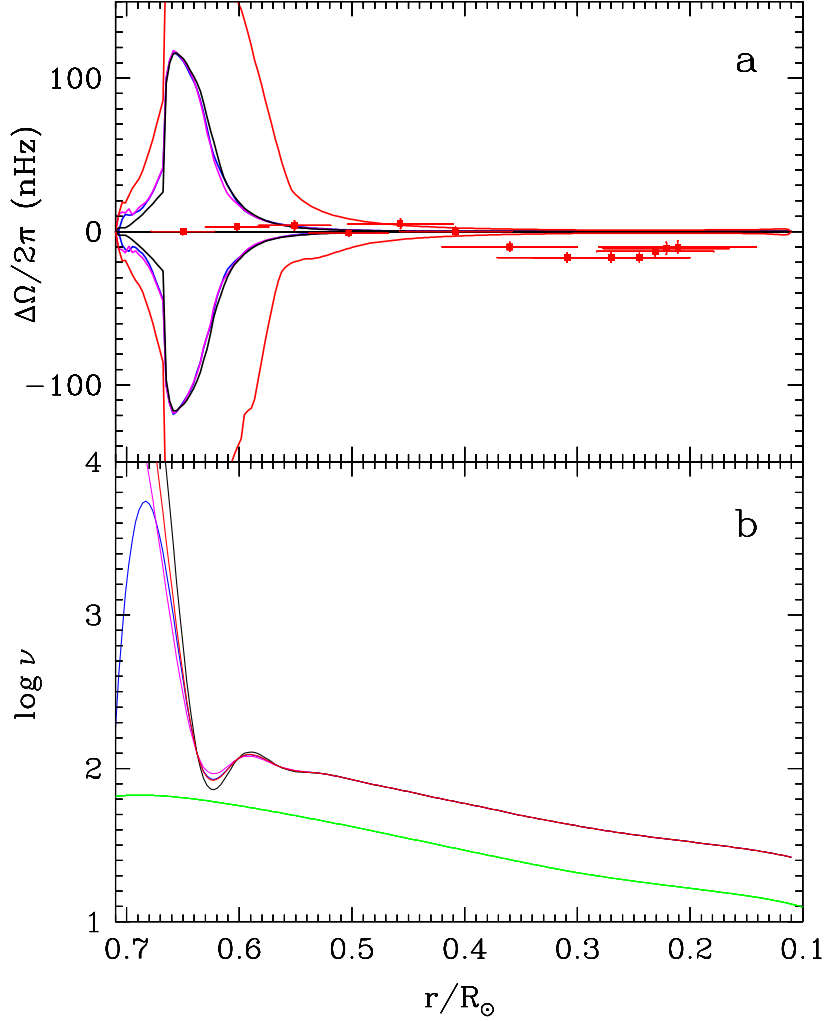


Fig. 7.— Same as in the previous figure but for spectrum (7) multiplied by the factor 2.7 (see text) and for the combined viscosity $\nu = \nu_v(f_v) + 2\nu_{\text{mol}}$. Exceptions are blue curves that were computed for $l = 1, 2, \dots, 7, 8$. In the expression (B2) for ν_v , the following parameters have been used: $f_v = 20$ (blue and purple curves) and $f_v = 10^3$ (black curve) for $0 \leq (r - r_c)/R_\odot \leq 0.04$, while $f_v = 0$ (all curves) for $(r - r_c)/R_\odot > 0.04$. For comparison, red curves are computed using spectrum (6).

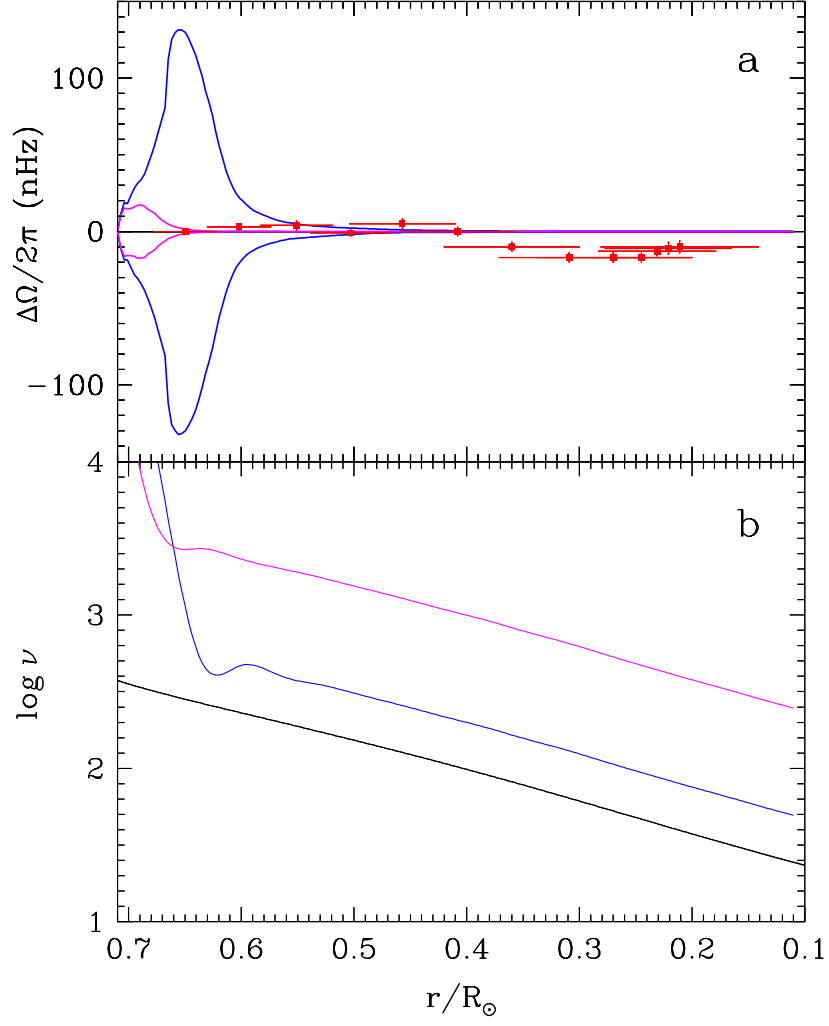


Fig. 8.— Same as in the previous figure but for spectrum (6) and for the combined viscosity $\nu = \nu_v(f_v) + f_{\text{mag}} \times \eta_{\text{mag}}$. In both cases, the parameter $f_v = 20$ has been used in the expression (B2) for $0 \leq (r - r_c)/R_\odot \leq 0.04$. Blue curve is computed with $f_{\text{mag}} = 2$, purple — with $f_{\text{mag}} = 10$. Black curve shows the magnetic diffusivity η_{mag} .